Available online at www.sciencedirect.com
ScienceDirect
International Journal of Heat and Mass Transfer 50 (2007) 36–44
International Journal of HEAT and MASS TRANSFER
www.elsevier.com/locate/ijhmt

An experimental investigation of natural convection with solidification in a differentially heated cavity

M.T. Stickland [a,*], T.J. Scanlon [a], J. MacKenzie [b]

[a] Department of Mechanical Engineering, University of Strathclyde, Glasgow G1 1XJ, United Kingdom
[b] Department of Mathematics, University of Strathclyde, Glasgow G1 1XJ, United Kingdom

Received 7 February 2005
Available online 20 September 2006

Abstract

This paper introduces an experimental rig used to produce data for the validation of computational models of natural convection within water in an enclosed cavity. The rig consisted of a rectangular cavity with the two long sides maintained at constant temperature. All other surfaces were insulated and adiabatic except for the top surface which was a free surface with an air gap between the free surface and the insulation. Experimental data in the form of velocity, ice growth rate and profiles are presented at 30 min time steps with a cold wall temperature of −10 °C and hot wall temperature of 5 °C. The data produced has systematic and random errors of ±0.4% and ±0.5%, respectively.

Keywords: PIV; Natural convection; Ice formation; Solidification

1. Introduction

The analysis of buoyancy-driven flows with coupled solid–liquid phase change is important in a broad range of scientific and engineering fields. Examples of these may be found in the solidification and melting phenomena commonly encountered in metallurgical processes, latent heat thermal energy storage, oceanography, food processing and nuclear reactor safety (see [1–3]). Such a case involving heat transfer with phase change coupled with a moving solid–fluid boundary is often referred to as a Stefan problem.

In the published literature, a substantial body of numerical and experimental work has been dedicated to the solution of Stefan problems in the presence of buoyancy-driven natural convection. Extensive reviews of such investigations may be found in the publications of Viskanta, [4], Yao and Prusa [5] and Prescott and Incropera [6]. However, the majority of the experimental work is of a qualitative nature, Braga and Viskanta [7], and there is a lack of suitable quantitative data that will allow the validation of computational fluid dynamics (CFD) codes which claim to be able to model the phase change phenomena.

The authors have created a rig which will allow the measurement of temperature and velocity in a quasi 2D cavity which has a heated wall opposite a cooled wall. All other surfaces are insulated and adiabatic apart from the free surface at the top of the cavity which had a 10 mm air gap between the free surface and the foam insulation. The free surface was unavoidable as the formation of ice causes the free surface to move upwards. However, this type of boundary condition is the norm for comparable experimental work. The experimental data generated from the rig and presented in this paper has additional interest as the temperature range contained the temperature at which the density inversion phenomenon occurs within water. This phenomenon leads to some interesting buoyancy-driven flow patterns and ice structures. The simplicity of the rig allowed the boundary condition of a numerical model to be easily defined and the data produced is readily applicable to the validation of the numerical models.

* Corresponding author. Tel.: +44 141 548 2842.
E-mail address: matt.stickland@strath.ac.uk (M.T. Stickland).

0017-9310/$ - see front matter © 2006 Elsevier Ltd. All rights reserved.
doi:10.1016/j.ijheatmasstransfer.2006.06.039

Nomenclature

A	aspect ratio ($=H/L$)
C_p	specific heat at constant pressure, J/kg K
H	height of liquid, m
k	thermal conductivity W/m K
L	length of cavity, m
Pr	Prandtl number
R	density distribution parameter
Ra	Rayleigh number
T	temperature, K
v	vertical component of velocity, m/s

Greek symbols

α	thermal diffusivity, m^2/s
β	thermal expansivity, K^{-1}
ρ	density, kg/m^3
μ	dynamic viscosity, N s/m^2
v	kinematic viscosity, m^2/s

Subscripts

c	cold
f	fusion
h	hot
m	maximum
r	reference
i	initial

The aim of this paper is to describe the experimental rig in detail and show a sample of the experimental data produced. The quality of the data is assessed through an error analysis.

2. Experimental rig

The experimental rig used consisted of a cavity 75 mm wide, 150 mm high and 150 mm deep with an aspect ratio, A, of 2. The vertical, opposite, sidewalls were integral heat exchangers. The end walls and bottom were created from 10 mm acrylic sheet to allow optical access. The top of the cavity was left open to create a free surface to allow for thermal expansion. The side wall heat exchangers were connected to two Grant Instruments (Cambridge) Ltd., R series, Low Temperature bath/circulators by insulated pipes through which circulated a mixture consisting of 50% glycol and 50% water. The constant temperature baths kept the coolant and side walls at a specified constant temperature within ±0.1 °C. Fig. 1 shows a photograph of the experimental rig with the refrigeration units, flow cavity, and heat exchangers. For clarity the insulation material had been removed from the cavity. In operation the rig was encased in 50 mm of expanded polystyrene foam. The heat exchangers which make up the hot and cold walls of the cavity were made of brass and had nine ducts machined within them through which the water/glycol coolant passed, Fig. 2. The inlet and outlet manifolds feeding these ducts had a variable diameter in order to ensure uniform flow rate through each duct. This ensured a uniform temperature and heat transfer rate on the surface of both heat exchangers. The design and heat transfer characteristics of the heat exchangers were modelled extensively using the Fluent CFD package in order to ensure the uniform temperature and heat transfer rate.

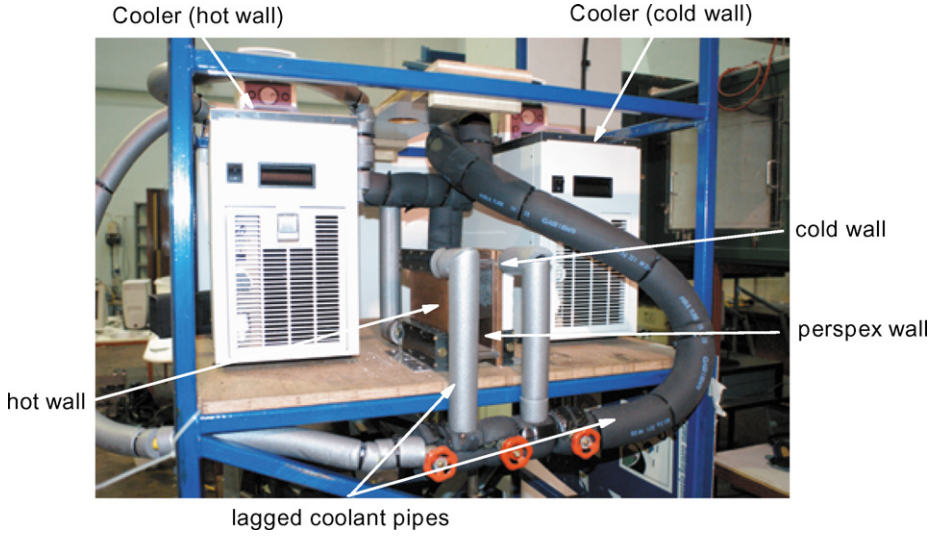

Fig. 1. Photograph of experimental rig.

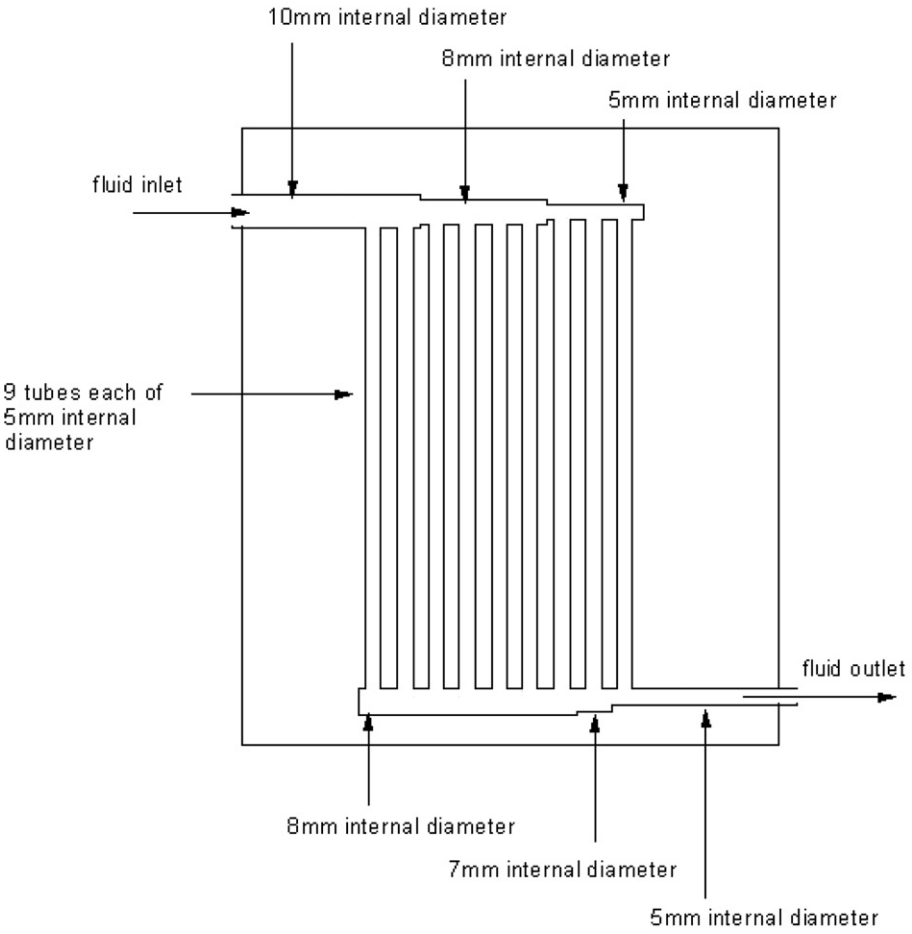

Fig. 2. Section through heat exchanger showing refrigerant ducts.

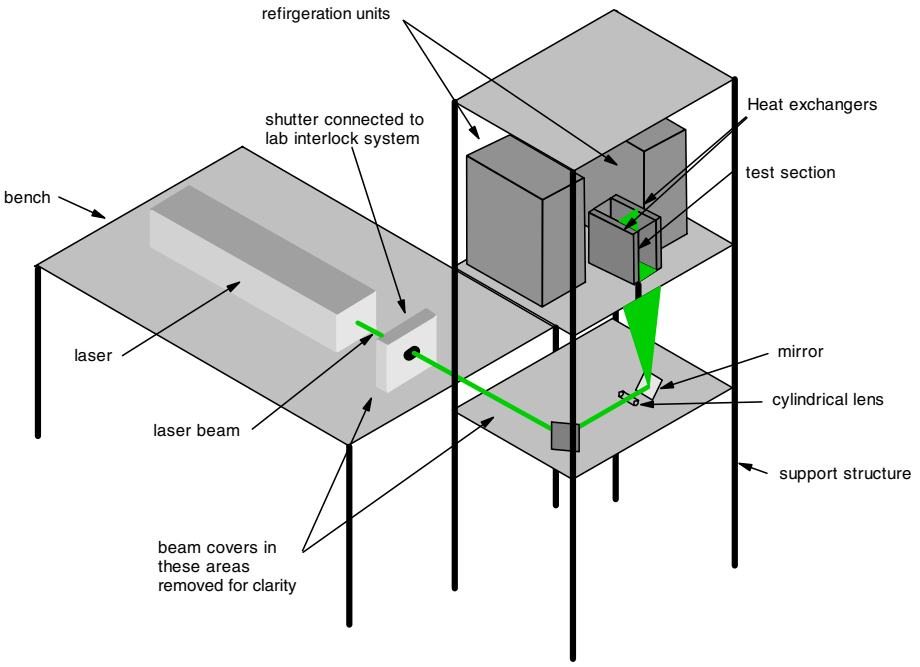

Fig. 3. Diagram of experimental rig showing optical path.

Fig. 3 shows a schematic of the rig and the optical path of the illumination laser. The Laser was a Lee Laser LDP-100MQG diode pumped Nd:YAG laser. The laser beam, with a wavelength of 532 nm, had variable pulse frequencies between 5 kHz and 50 kHz with energy per pulse in the range of 1–8 mJ per pulse. For this experiment the laser was run at 40 kHz thereby producing a quasi continuous wave laser with a nominal power of approximately 40 W. The beam was expanded into the cavity to form a 2D illumination sheet approximately 2 mm thick. For the majority of the experiment the laser shutter remained closed and was only opened for the time required to acquire the images of the flow field to avoid problems with the laser heating the working section. The camera used to acquire the images of the flow field was a Photron Ultracam high speed digital video system running at 60 frames per second with a resolution of 1024 × 1024 pixels. The camera head was fitted with a Nikon 60 mm lens and a 570 nm high pass filter.

2.1. Experimental procedure

To ensure high repeatability of the experiments and to ensure that the initial boundary conditions of the experiment were well defined, in order to allow successful numerical modelling of the flow, the procedure at the start of the experiment was strictly adhered to. Before any fluid was introduced into the rig the refrigeration units were switched on and set to the hot and cold wall temperatures. The rig was then surrounded in insulation and allowed to reach equilibrium. When the rig was found to be in thermal equilibrium the seeding, neutrally buoyant 80–120 μm diameter fluorescent ballotini from John Hopkins University, was placed into the bottom of the test chamber and distilled water which had been cooled to the temperature of the hot wall siphoned into the rig to a depth of 140 mm to avoid the inclusion of air bubbles in the rig. The top 10 mm of the rig was left empty to allow for the expansion of the water as the ice formed on the cold wall. The siphoning process took approximately 30 s and was sufficient to mix the seeding thoroughly into the water. The repeatability of the experiment, as discussed in Section 3.1.4, implies that variability of the initial boundary conditions caused by the siphoning of the water into the rig had little effect on the results of the experiment. The insulation on the upper surface was replaced when the water had been placed in the rig. When data were to be acquired the shutter on the laser was opened, the insulation on the viewing window was removed, the camera triggered and 512 images acquired. When the images had been acquired the shutter on the laser was closed, condensation that had formed on the viewing window was removed and the insulation was replaced. The total time elapsed for acquisition of the data from opening to closing the laser shutter was less than twenty seconds. Data were acquired at ten minute intervals. At the end of the experiment a laminated section of graph paper was placed in the plane of the laser sheet and photographed to create a datum from which the linear dimensions of the PIV analysis could be determined. Subsequent to the data acquisition the images were analysed by DANTEC FlowManager PIV software.

Table 1
Experimental conditions

Hot wall temperature, T_h	5 °C
Cold wall temperature T_c	−10 °C
Fluid	Distilled water
Initial water temperature, T_i	5 °C
Rayleigh number, *Ra*	1.6×10^7
Prandtl number, *Pr*	12.32

2.2. Boundary conditions

This paper contains data for one set of boundary conditions which are shown in Table 1. The Rayleigh number was obtained using

$$Ra = \frac{g\beta(T_h - T_f)H^3}{\nu\alpha}. \quad (1)$$

The fluid properties were taken from Çengel [8] at the median temperature of the fluid, 2.5 °C

$$g = 9.81\ \mathrm{m/s^2}, \quad H = 0.14\ \mathrm{m}, \quad \beta = -2.65 \times 10^{-5}\ \mathrm{K^{-1}},$$
$$\nu = 1.66 \times 10^{-6}\ \mathrm{m^2/s}, \quad \alpha = 1.34 \times 10^{-7}\ \mathrm{m^2/s},$$
$$T_h = 5\ ^\circ\mathrm{C}, \quad T_f = 0.01\ ^\circ\mathrm{C}.$$

The Prandtl number

$$Pr = \frac{\mu C_p}{k}, \quad (2)$$

where $C_p = 4.211$ kJ/kg K, $k = 0.566$ W/m K, $\mu = 1.656 \times 10^{-3}$ kg.

3. Results and discussion

This paper contains the results for one set of boundary conditions in order to demonstrate the capability of the experimental rig and the quality of the data produced.

3.1. PIV analysis

The images analysed with DANTEC FlowManager software were 1024 × 1024 pixels analysed with an interrogation area of 32 × 32 pixels by cross correlation. Prior to analysis the images were masked so that the area outside of the experimental chamber produced null vectors. A sample of the vector maps produced may be seen in Fig. 4.

3.1.1. Cross correlation PIV

Cross correlation PIV is a non-intrusive method of measuring the velocity vectors in a fluid flow. To measure the velocity vectors the displacement of small, neutrally buoyant seeding particles in the flow field are measured. To acquire 2D velocity vectors the flow field is usually

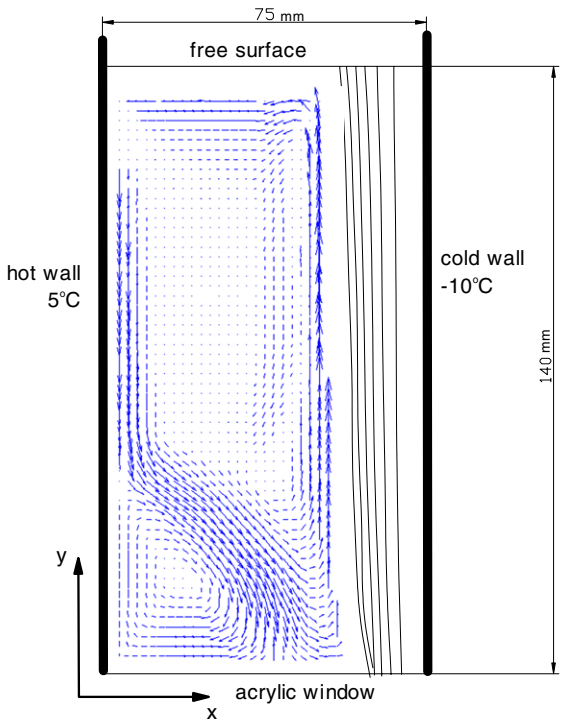

Fig. 4. Typical vector map produced by the FlowManager software. Flow chamber dimensions including coordinate system, hot and cold wall temperatures, ice front positions at 10-min intervals and vector map of flowfield after 60 min.

illuminated by a thin sheet of laser light. If the surrounding light levels are kept low then only the particles in the 2D slice of the flow field, illuminated by the laser, will be visible. If two photographs of the 2D light sheet are taken separated by a small time interval then, by analysing a small region of the two photographs, it is possible to determine the magnitude and direction of the displacement of the particles in the interrogation region. Knowing distance, time and direction of motion of the particles in the interrogation region the velocity vector of the fluid at the point in the flow field may be inferred. If the images are subdivided into a number of interrogation regions then the velocity vectors within the illuminated region of the flow field may be determined. For a more detailed explanation of PIV analysis see Raffel et al. [9].

3.1.2. Determination of cross correlation time step

The PIV images were acquired by high speed digital camera at 60 frames per second with exposure times of 1/250th of a second with 512 images stored at each datapoint. It was therefore possible to carry out multiple cross correlation analyses over different time steps at each data point. The Rayleigh number of the flow within the cavity indicated that the flow within the cavity was laminar. It was therefore possible to use a statistical analysis of the velocity measured in the vessel to determine the quality of the measured data. Laminar flow should, theoretically, have zero standard deviation if the flow was steady state. As the flow field within the vessel was considered to be quasi steady state high standard deviation would imply errors in the cross correlation technique due to an error in the selection of the time step between images. Fig. 5 shows the effect of the time step on the vertical component of the velocity calculated at a point in the centre of the cavity within the high speed flow field and also the effect of time step on the standard deviation.

The standard deviation was found to drop significantly as the time step was increased and the calculated velocity became constant. It was therefore decided to use a time step of 1.333 s which corresponded to cross correlating images separated by 80 frames. Thus, the data presented in this paper, had a standard deviation of approximately 0.002 mm/s in the high speed flow within the body of the chamber and a standard error of ± 0.0008 mm/s corresponding to a standard deviation of 0.8% and standard error of $\pm 0.4\%$. Combined with this estimate of the random uncertainty in the data consideration must also be given to the systematic gain uncertainty included in the data due to the measurement of the scale used to obtain a linear dimension for the PIV analysis. It was estimated that this was of the order $\pm 0.5\%$. The low standard deviation within the data was not unexpected as the work of Gebhart et al. [10] suggested that transition to turbulent convective flow within a cavity should not occur until a Rayleigh number of 10^9.

3.1.3. Data quality

It should be noted that all vector maps, including the one shown, consisted of the raw vectors acquired from the initial cross correlation analysis. This shows that the data acquired was of high quality as the vector plots were not obtained by post processing. Post processing of vector data sets is quite common when undertaking PIV analysis. There are a number of ways the vectors, created by the cross correlation can be post processed. In each case the aim of the post processing is to identify any velocity vectors that might have been calculated in error. These errors could be due to a lack of seeding particles in the interrogation region, particles moving out of the interrogation region between successive images or the presence of high velocity gradients within the interrogation region. When the error vectors are identified they can be replaced by a vector created by interpolation of the surrounding vectors. Further information about data validation and replacement techniques may be found in the work of Raffel et al. [9].

3.1.4. Repeatability

In order to assess the repeatability of the experiment it was repeated three times with the same initial boundary conditions. Fig. 6 shows three plots of the v component of the velocity vector at a height of 70 mm after 60 min taken from the three experiments. It may be seen that the data from repeating the experiment three times shows good agreement proving that the repeatability of the experiment

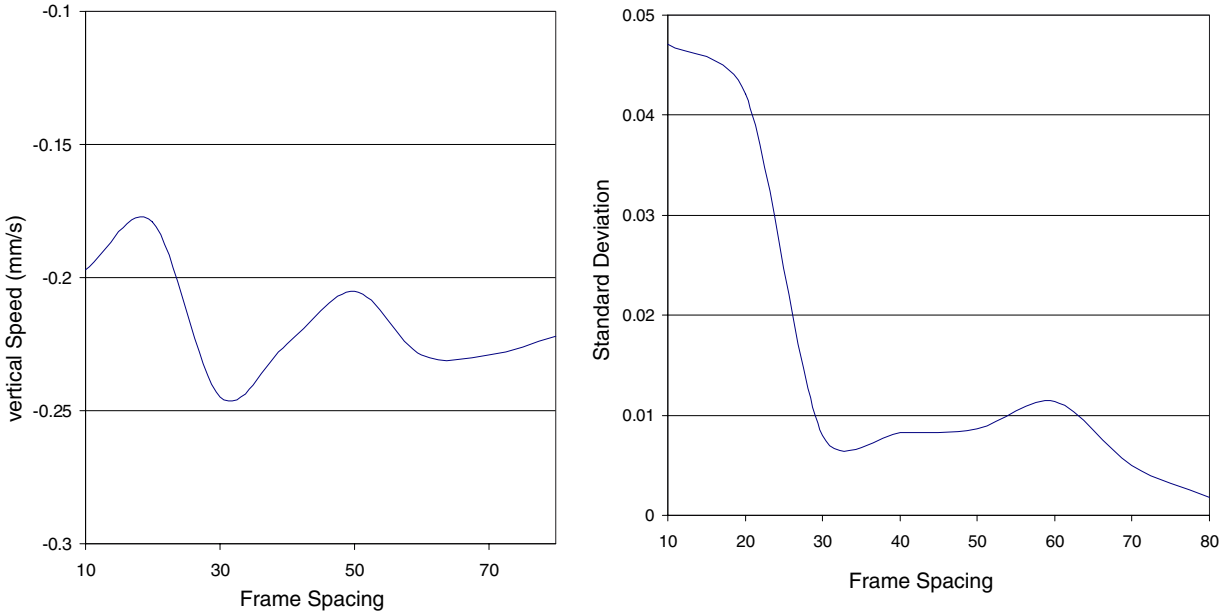

Fig. 5. Effect of time step on calculated velocity.

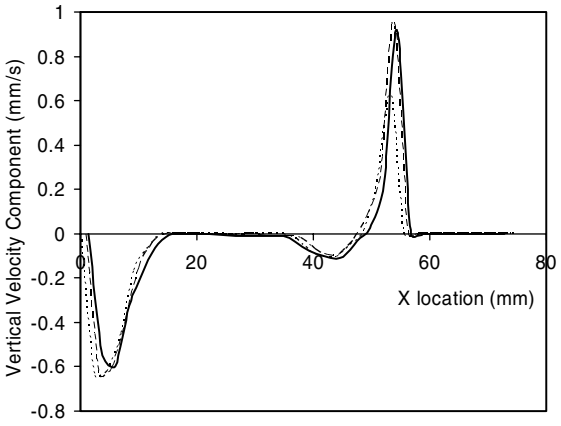

Fig. 6. Repeatability plot, 60 min, $y = 70$ mm.

was acceptable. The slight disparity between the shear layer velocity profiles on the right hand wall in one dataset was thought to be due to the analysis mesh not capturing the high velocity peak in this one case.

3.2. Streamlines

Fig. 7 shows the streamlines within the flow field after 30, 60 and 90 min. It may be seen that they highlight the effect of the density extremum on the flow field. Water has the unique property that the maximum density does not exist in the solid phase but, at atmospheric pressure, occurs at approximately 4 °C. Thus, at the top of the hot wall the water, cooled by the cold wall, had a temperature below 4 °C. The hot wall heated the water, its density increased, and caused the water to descend due to the negative buoyancy. As the water descended it was heated, its temperature rose and reached the temperature for maximum density consequently the flow started to experience positive buoyancy. The water cannot rise, due to the fluid descending towards it and was therefore forced to separate from the wall. This created a recirculation region at the bottom of the hot wall. The water, when it had separated from the cold wall was forced to the cold wall where its temperature was decreased. Because the temperature falls below the extremum temperature the cooling of the water caused the density to reduce and the fluid to rise up the cold wall before recirculating to the hot wall.

In the recirculation region, in the lower left quadrant, the temperature of the water was maintained above the extremum temperature and the conventional thermal convection currents were created. The water close to the hot wall was heated, the density fell causing the water to rise. However, the rising water met the fluid below the extremum temperature flowing down the wall and was also forced to separate. As the experiment progressed it was noted that the separation point moved progressively down the hot wall. The gradual cooling of the bulk of the fluid within the vessel decreased its temperature below the extremum temperature from the initial temperature of 5 °C. The cooling of the majority of the fluid caused the temperature of the fluid as it reached the top of the hot wall to decrease with time. As the temperature of the water at the top of the hot wall decreased, the length of the hot surface over which the fluid needed to flow before reaching the extremum temperature increased. This caused the separation point to move down towards the bottom of the vessel.

3.3. Velocity profiles

A plot of the vertical, v, component of the velocity vector at three heights within the chamber after 30, 60 and 90 min

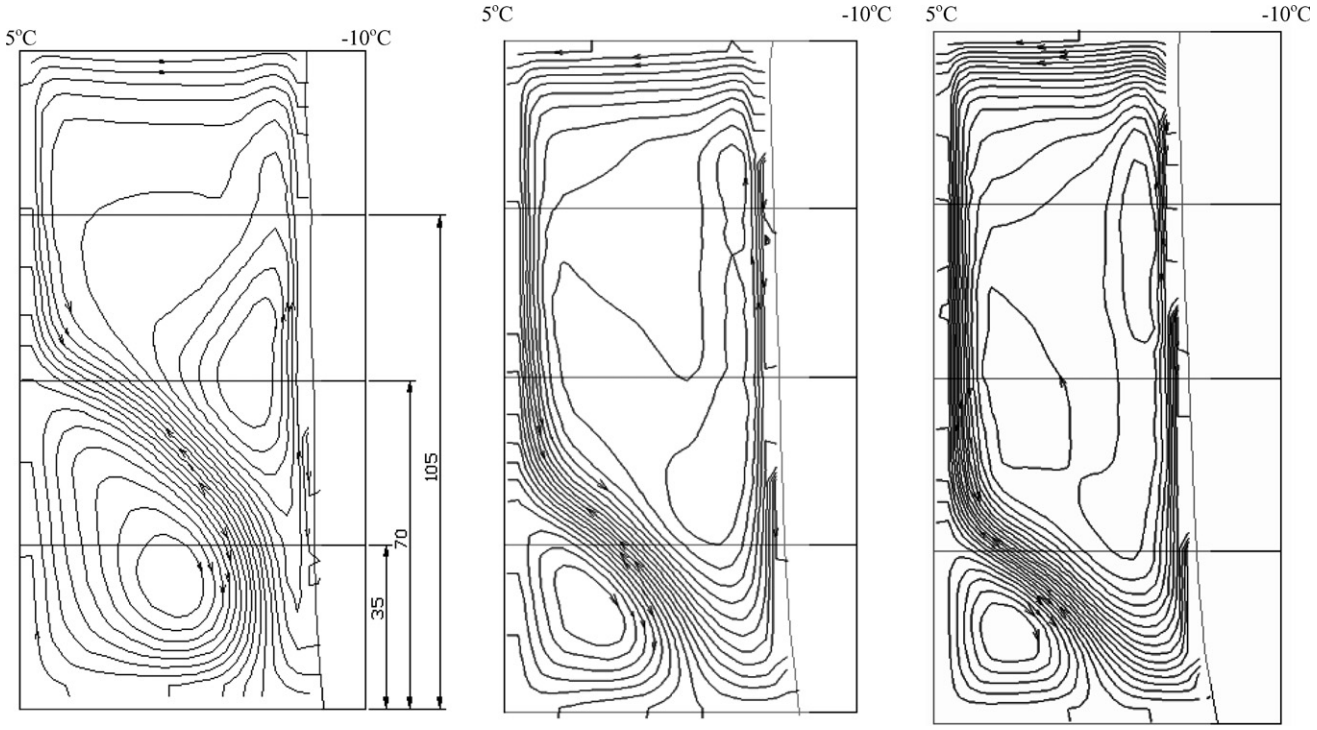

Fig. 7. Streamline at, from left to right, 30, 60 and 90 min.

may be seen in Figs. 8–10, respectively. The position of the separation point on the hot wall may be determined by considering the v component of the velocity. On the upper part of the wall the heating of the fluid caused a flow down the wall and a negative v component of the velocity vector was measured. On the lower part of the wall the heating of the fluid caused the fluid to rise and a positive v component of the velocity to be measured. Where the two flows meet and separate a zero v component of the velocity vector was determined. From Fig. 8 it may be seen that, at 30 min, the separation point, shown by the zero v component of the velocity, existed 70 mm from the base of the cavity on the hot wall. Above this point the velocity was negative and below was positive. Fig. 9 shows that, after 60 min, the velocity on the hot wall at 35 mm was positive and the velocity at

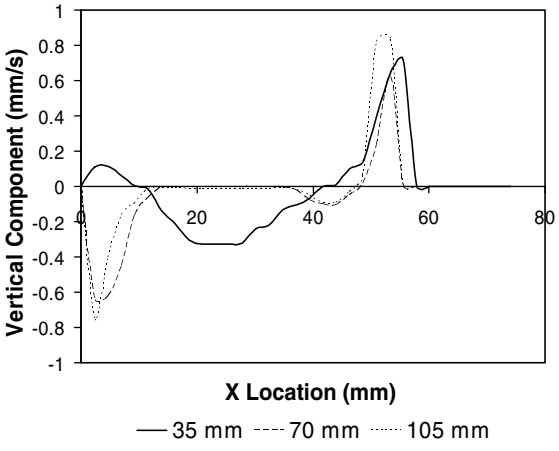

Fig. 9. Vertical component of velocity at 60 min.

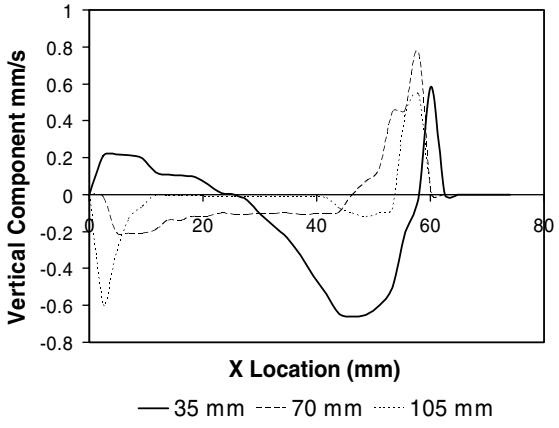

Fig. 8. Vertical component of velocity at 30 min.

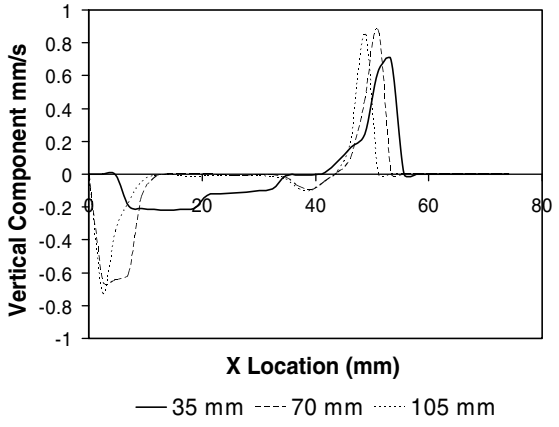

Fig. 10. Vertical component of velocity at 90 min.

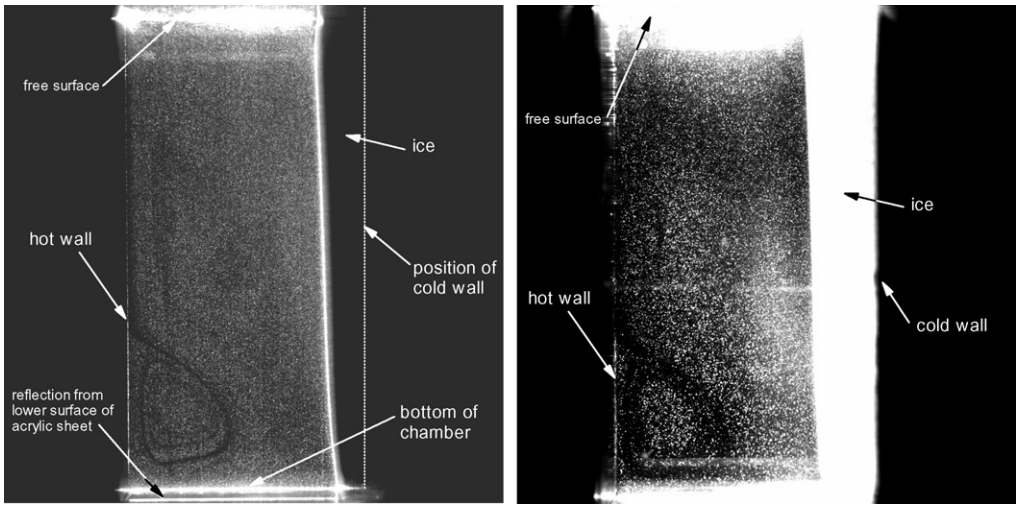

Fig. 11. PIV images.

70 mm was negative indicating that separation point had dropped below mid height. Fig. 10 shows that, at 90 min, the separation point existed at 35 mm above the bottom of the cavity. In Figs. 8–10 it can be seen, from the increasing region of zero flow toward the right of the cavity and the displacement of the high velocity peaks on the cold wall towards the centre of the chamber, that the thickness of the ice sheet on the cold wall increased with time.

3.4. Ice thickness

The growth of the ice sheet on the cold wall of the chamber was determined from the PIV images, a sample of such an image may be seen in Fig. 11. Both images were acquired after 60 min. However, the image on the left of Fig. 11 shows the image of the flow field acquired through a 570 nm high pass filter which removed the reflected laser light and allowed only the fluorescent light from the seeding particles to pass to the camera sensor. It may be seen in this image that the ice front shows up as a distinct thin line where the fluorescent light is reflected from the surface of the ice sheet. The appearance of two lines at the bottom of the chamber is due to the laser sheet passing through fluorescent seeding which has precipitated to the bottom of the vessel and the reflection of this light from the lower surface of the acrylic sheet that makes up the bottom of the chamber. The figure on the right shows the same flow field with the filter removed and illustrates why the images viewed through the high pass filter were used. In this case it may be seen that the reflected laser light from the surfaces of the chamber and the ice sheet caused considerable glare which introduced significant noise into the data contained within the image. In order to determine quantitative data about the position of the front of the ice sheet the images were imported into AutoCAD and scaled from known dimensions on the images. A line was then fitted through the ice front and the location of the line and hence the ice front within the cavity was determined. Fig. 12 shows

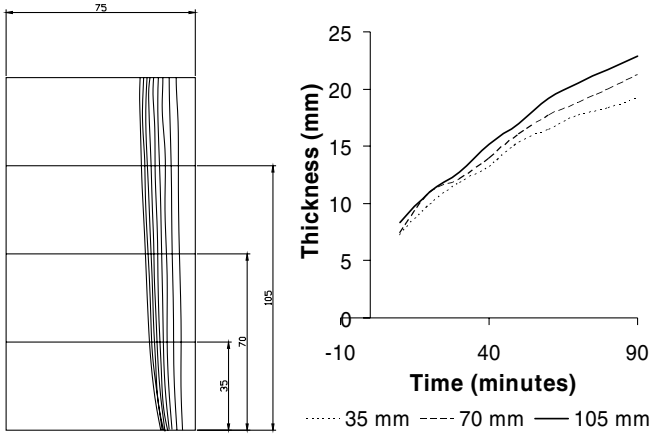

Fig. 12. Ice profiles and ice thickness.

the position of the ice front at ten minute intervals and also shows the ice thickness at three heights within the chamber during the experiment. It may be seen that the ice growth rate decreased with time as the layer of ice created an insulating surface over the cold heat exchanger. The ice thickness was not constant up the plate but increased in thickness with height. At the top of the ice sheet it may be seen that there was a slight reduction in the ice growth rate due to the presence of the free surface of the water and the small air gap between the free surface and the upper layer of insulating foam.

4. Conclusion

This paper has shown that an experimental facility has been created which allows the quantitative measurement of the flow field in a cavity driven by natural convection. Vector maps were produced and velocity profiles at three heights within the chamber presented. The formation of the ice sheet on the cold wall of the cavity was measured and ice front profiles and sheet thickness presented. The

data produced allowed the flow field within the cavity to be discussed and this highlighted the effect the phenomenon of the density extremum within liquid water has on the convective flow patterns at this temperature. The rig produced high quality data which showed good repeatability and accuracy. The boundary conditions of the experiment were well defined such that the data produced are ideal for validation of numerical models of the so called Stefan problem.

References

[1] R.J. Goldstein, J.W. Ramsey, Heat transfer to a melting solid with application to thermal energy storage systems, in: J.P. Hartnet et al. (Eds.), Studies in Heat Transfer: A Festschrift for E.R.G. Eckert, McGraw-Hill, Washington, DC, 1979, pp. 199–208.

[2] S. Ostrach, Fluid mechanics in crystal growth, ASME J. Fluids Eng. 105 (1983) 5–20.

[3] D. Feldman, M.M. Shapiro, D. Banu, C.J. Fuks, Fatty acids and their mixtures as phase-change material for thermal energy storage, Solar Energy Mater. 18 (1989) 201–216.

[4] R. Viskanta, Natural convection in melting and solidification, in: S. Kakac et al. (Eds.), Natural Convection: Fundamentals and Applications, Hemisphere, Washington, DC, 1985, pp. 845–877.

[5] L.S. Yao, J. Prusa, Melting and freezing, Adv. Heat Transfer 19 (1989) 1–95.

[6] P.J. Prescott, F.P. Incropera, Convection heat and mass transfer in alloy solidification, Adv. Heat Transfer 28 (1996) 231–338.

[7] S.L. Braga, R. Viskanta, Effect of density extremum on the solidification of water on a vertical wall of a rectangular cavity, Exp. Thermal Fluid Sci. 5 (1992) 703–713.

[8] Çengel Heat Transfer, McGraw-Hill International, ISBN: 0-07-0115223-7.

[9] M. Raffel, C. Willert, J. Kompenhans, Particle Image Velocimetry, Springer, Berlin, 1998, ISBN 3-540-63683-8.

[10] B. Gebhart, Y. Jaluria, R.L. Mahajan, B. Sammakia, Buoyancy Induced Flows and Transport, Hemisphere, New York, 1988.